Journal of Materials Chemistry A

Accepted Manuscript

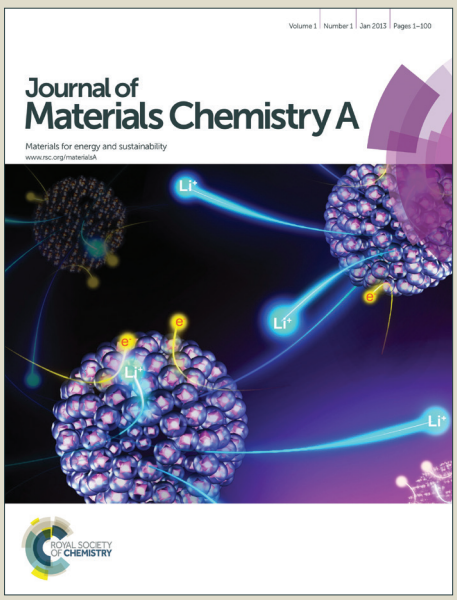

ROYAL SOCIETY OF CHEMISTRY

www.rsc.org/materialsA

Journal Name

COMMUNICATION

Hierarchical nanostructured nickel cobalt oxides microspheres composed of mesoporous nanothorn array and their superior rate capability as anode materials for lithium ion batteries

Received 00th January 20xx,
Accepted 00th January 20xx

DOI: 10.1039/x0xx00000x

www.rsc.org/

Zhen-Dong Huang [a],* Kun Zhang [a], Ting-Ting Zhang [a], Xue Li [a], Rui-Qing Liu [a], Xiao-Miao Feng [a], Yi Li [a], Xiu-Jing Lin, [a] Yan-Bing He [b], Xu-Sheng Yang [c] and Yan-Wen Ma [a],*

Hierarchical nickel cobalt oxides (NCO) microspheres comprised of nanoscale mesoporous thorn arrays are developed as superior rate high capacity anode in this work, i.e. 1063.3 and 860 mAhg^{-1} at 180 and 4500mAg^{-1}, respectively. Stoichiometric urea is served as self-template to favor the self-assembling of well-organized $NiCo(OH)_2CO_3$ thorn microspheres precursor under an optimized hydrothermal reaction. The dispersed multi-phase hybrid crystal structure and the favorable specific surface area obtained during the controlled pyrolysis of $NiCo(OH)_2CO_3$ microspheres markedly promote the cyclic stability of the single phase $Ni_{1.5}Co_{1.5}O_4$.

The impressive characteristics including relatively high energy density, cyclic stability and environmental benignity make rechargeable lithium ion batteries (LIBs) dominate the energy storage market and become the most important energy storage system to keep solar and wind energy and power sources to power different portable electronic devices, electric tools and electric vehicles.[1] To satisfy these ever-growing demands, the design and synthesis of new attractive nanostructured electrode materials have become one of the key strategies to promote the lithium ion storage properties, especially rate capability of LIBs.[1,2]

As one of the pivotal components of LIBs, the electrochemical performance of LIBs highly depends on the capacity, rate capability and cyclic stability of anode materials. [3] Amongst the available materials, carbonaceous materials still dominate the industrial anode market because of their relatively better cyclic stability. However, their inherent low theoretical specific capacity of carbon (372 mAh g^{-1}) limit the further improvement of energy density of LIBs. [4] Transition metal and their oxides, have been considered as promising alternative anode materials, owing to their much larger theoretical capacity. [5-8] Nevertheless, their rate capability and cyclic stability are still required to be further improved due to the slow kinetics of electrochemical conversion reaction and the significant volumetric expansion during the charge and discharge cycling of Li ions and other side reactions.

Recently, binary transition metal oxides, such as $A_xB_{3-x}O_4$ (A and B =Co, Ni, Mn, Zn or Fe), have attracted intensive attention as promising anode materials for next-generation LIBs for their inherited characteristics of high capacity and low cost.[9-20] Synergistically binary metal oxides present enhanced electrical/ionic conductivity, reversible capacity, mechanical stability, and so on, which are superior to single-component metal oxides. Binary $ZnFe_2O_4$,[9] $ZnMn_2O_4$,[10] $ZnCo_2O_4$,[11, 12] $NiCo_2O_4$,[13] and $MnCo_2O_4$,[14-19] with different nanostructures have been developed as advanced anode materials for LIBs. Lately, Major attention have been paid to synthesize the nanostructured $Co_xMn_{3-x}O_4$, in which x/(3-x)=1/2 or 2/1, and to modify their structure and electrochemical performance. Until now, only few work reported the synthesis and electrochemical performance of the nanostructured $Co_xMn_{3-x}O_4$, in which x/(3-x)=1/1. An interesting hierarchical flower-like $Ni_{1.5}Co_{1.5}O_4$ nanostructures were just reported as a high capacity (980.8 mAhg^{-1} after 30 cycles under 100 mAg^{-1}) anode materials, which were synthesized by a hydrothermal method without any template, catalyst and surfactant, followed by a calcinating process.[20] Unfortunately, further work are required to promote the rate and cyclic performance of $Ni_{1.5}Co_{1.5}O_4$.

As far as we know, it is one of the attractive strategies to prepare nanostructured transition metal oxides through thermally pyrolyzing their corresponding nanostructured carbonates or basic carbonates precursors under optimized conditions. [11-13, 21-23] Therefore, it is very important to control the shape and composition of the precursor, because it would highly influence the morphologies and atomic compositions of final metal oxides. Nowadays, the hydro/solvothermal synthesis of the carbonates using urea as both precipitator and self-template has been considered as one of the state-of-the-art ways. [21-23] Without using any additional surfactant or templates, the morphologies of the target carbonates can be effectively controlled by precisely adjusting the type of used

[a] Address here.
[b] Address here.
[c] Address here.
† Footnotes relating to the title and/or authors should appear here.
Electronic Supplementary Information (ESI) available: [details of any supplementary information available should be included here]. See DOI: 10.1039/x0xx00000x

reaction solvents, the applied concentration of both urea and transition metal salts and the molar ratio of transition metal/urea, as well as the reaction temperature and duration. For example, $Co_2(OH)_2CO_3$ nanosheets, [21] dumbbell-like micro-sphere $Ni_{1/3}Mn_{1/3}Co_{1/3}CO_3$, [22] and $Mn_{0.54}Ni_{0.13}Co_{0.13}$ $(CO_3)_{0.8}$ solid sphere, [23] were assembled with the aid of saturated urea at different conditions for further applications.

In view of above concerns, in this work, a scalable hydrothermal method (see supplementary information) was designed to assemble an uniform hierarchical binary basic nickel cobalt carbonate $NiCo(OH)_2CO_3$ nanothorn spheres as precursors for preparing the target binary nickel cobalt oxides (NiCoOx, marked as NCO) hierarchical porous-thorn sphere via a short low temperature annealing process. Benefitted from their unique morphology and structure, the obtained NCO nanostructures deliver superior rate capability and greatly promoted cyclic stability as advanced anode materials for LIBs comparing to the work reported in reference [20]. The effects of annealing temperature on the morphology, crystal structure and in turn Li-ion storage properties of the final NCOs are closely studied in this report.

The uniform nanothorn spheres morphology and monoclinic crystal structure of self-assembled binary basic nickel cobalt carbonate $NiCo(OH)_2CO_3$ are given in Figs. 1 and S1. The diameter of the secondary spheres are about 4 - 8 µm. The diameters of the smooth thorns are ~100 nm. As shown in Fig. 1c, the X-ray diffraction (XRD) pattern of self-assembled products is matched well with that of reported monoclinic cobalt hydroxycarbonate. [21] This observation confirms that the obtained precursor is monoclinic binary $NiCo(OH)_2CO_3$.

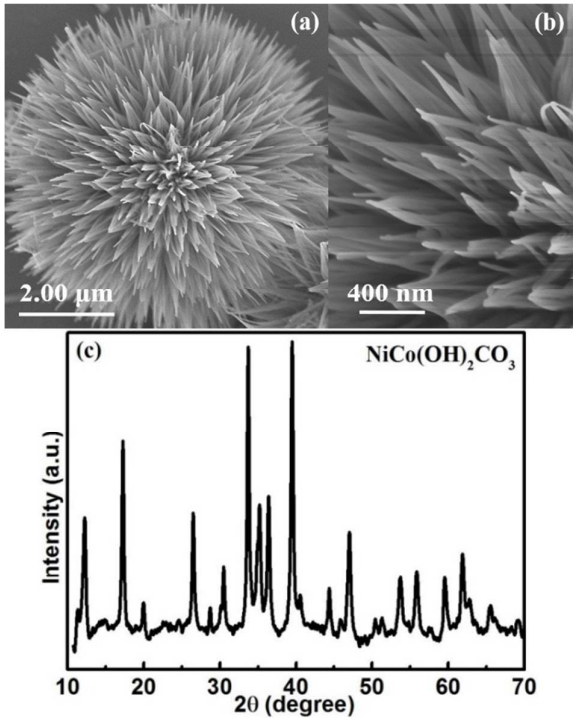

Fig. 1. The morphology (a, b) and X-ray diffraction pattern (c) of as-prepared $NiCo(OH)_2CO_3$ precursor

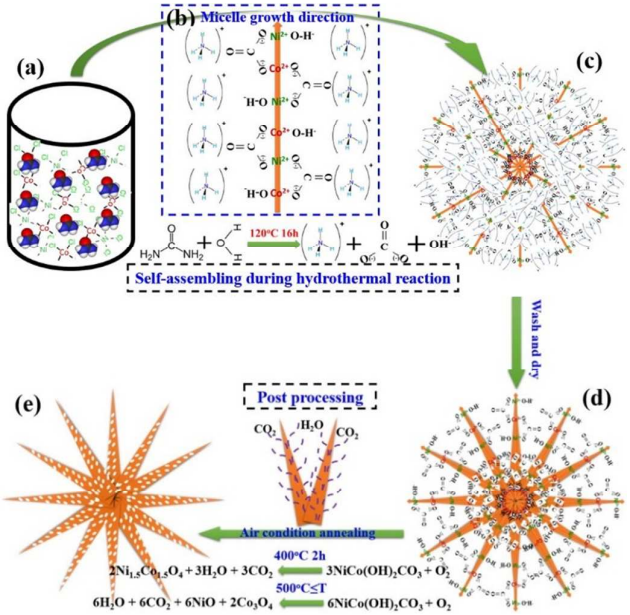

Fig. 2. Schematic illustration of the typical self-assembling strategy of hierarchical nanostructured $NiCo(OH)_2CO_3$ nanothorn spheres and the post processing for the preparation of final NCO sphere nanostructure with porous nanothorn array: (a) mixed clear solution of urea, $CoCl_2$ and $NiCl_2$, (b) the proposed self-assembled primary micelle, (c) the proposed self-assembled spherical thorn micelle, (d) the proposed hierarchical nanostructured $NiCo(OH)_2CO_3$ nanothorn sphere, (d) the proposed schematic of NCO porous nanothorn sphere.

The reaction mechanisms behind the self-assembling process of hierarchical $NiCo(OH)_2CO_3$ nanothorn spheres are schematically elaborated in Fig. 2. At the beginning of hydrothermal reaction, urea molecules reacts with water molecules and generate high concentration carbanions, hydroxyl and ammonium radical, meanwhile, the generated radical species and Ni^{2+} and Co^{2+} tend to self-assemble into one dimensional primary micelles via electrovalent bond and hydrogen bond, as illustrated in Fig. 2b. During the hydrothermal reaction, one end of the just formed nearest neighbouring 1D micelles grow towards the core and gather together to form low energy spherical nucleus due to the trend towards decrease of Gibbs free energy of the whole system. In the same time, another end of the 1D micelle grow continuously along with the diameter direction of self-assembled spherical nucleus to form secondary spherical micelles as proposed in Fig. 2c. After removing the soluble ammonium radical and Cl^- by washing with distilled water for 3 times, the final nanostructured $NiCo(OH)_2CO_3$ spheres comprised of the well-organized nanothorn arrays, see Figs. 1a and 2d, can be obtained. High resolution SEM image shown in Fig. S1b is the direct and powerful support of self-assembling mechanisms proposed above.

Subsequently the as-prepared hydrocarbonates were used as precursors to prepare the target binary nickel cobalt oxides ($NiCoO_x$, marked as NCO) hierarchical porous spheres composed of nanothorn arrays by a short post heat treatment

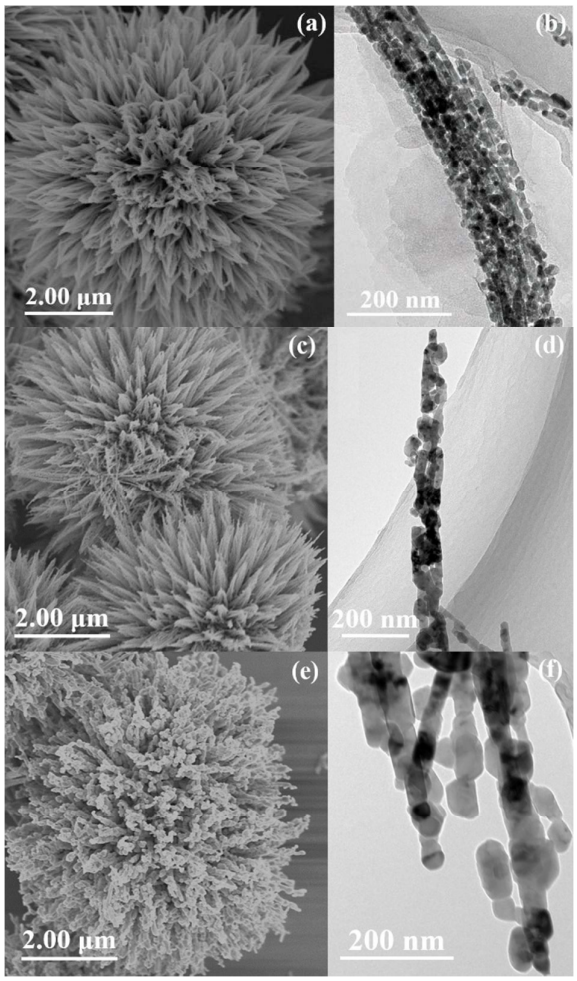

Fig. 3. The low magnification SEM images and high resolution transmission electron microscope (FE-TEM) images of (a, b) NCO-400, (c, d) NCO-500, and (e, f) NCO-600, respectively.

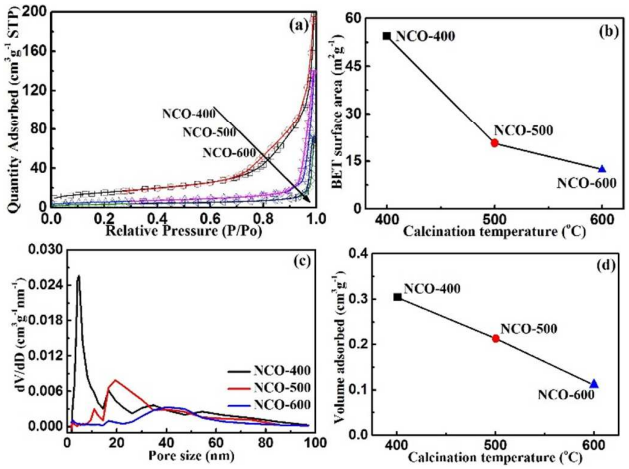

Fig. 4. (a) The nitrogen adsorption/desorption isotherm (a) and the BET specific surface area (b) of hierarchical nickel cobalt oxides varied with calcination temperature, (c) the pore-size distribution curve and (d) the pore volume of hierarchical nickel cobalt oxides varied with calcination temperature.

at a low temperature. As illustrated in Fig. 2d and 2e, the monolithic $NiCo(OH)_2CO_3$ nanothorns become porous thorns integrated by nanosized $Ni_{1.5}Co_{1.5}O_4$ particles due to the generation of large amount of CO_2 and H_2O gas when $NiCo(OH)_2CO_3$ decomposes during the calcination process. Finally, the hierarchical nanostructured NCO spheres formed with porous nanothorn array as proposed in Fig 2e are obtained, see Figs. 3 and S2. Similar phenomenon was also reported in Zhou's recent work. [21] In order to optimize the morphology, crystal structure and in turn the electrochemical performance of final nickel cobalt oxides, the $NiCo(OH)_2CO_3$ hierarchical precursors were annealed at 400, 500 and 600 °C for 2h, respectively. The corresponding products are marked as NCO-400, NCO-500 and NCO-600, respectively.

As shown in Figs. 3 and S2, when the calcination temperature increase from 400 to 600 °C, the sizes of primary oxide particles grow from several nano-meters to around 40 nm, meanwhile, the microstructural morphology of obtained NCOs gradually changes from the integrated mesoporous thorn bundles array of NCO-400 to stone-pillar-like mesoporous thorn array of NCO-600. Fortunately, the secondary particles still keep the sphere-like hierarchical nanostructure, see Fig. S2. The nitrogen adsorption/desorption isotherm and pore-size distribution curves present in Fig. 4 confirm the mesoporous characteristics of NCOs thorn sphere. The calculated Brunauer–Emmett–Teller (BET) specific surface area of NCO-400, NCM-500 and NCM-600 are 54.364, 20.553 and 12.374 m^2g^{-1}, respectively. The average pore size of NCO-400, NCM-500 and NCM-600 increase from ~ 4.8 nm to 19.38 and 40 nm with the increase of calcination temperature from 400 °C to 500 and 600 °C, see Fig. 4b. The nano-sized primary particles and the special mesoporous hierarchical structure could provide short diffusion distance and large active area for Li^+.

The evolution of crystal structure of NCO-400, NCO-500 and NCO-600 were analysed via X-ray diffraction (XRD). As shown in Fig. 5, the obtained XRD pattern of NCO-400 can be indexed to a pure face-centered-cubic (fcc) phase, like $NiCo_2O_4$ (a=8.269 Å; space group Fd3m (227), JCPDS no. 73-1702), in which nickel ions occupy the octahedral sites and cobalt ions are distributed over both octahedral and tetrahedral sites. It is now manifest that NCO-400 is mesoporous $Ni_{1.5}Co_{1.5}O_4$ hierarchical thorn spheres. As desired, the cubic NiO phase (JCPDS no. 65-2901) can be indexed from XRD patterns of both NCO-500 and NCO-600, as indicated by the stars in Fig. 5. This observed phenomenon, similar to that observed by Li et al, should be caused by the decomposition of $Ni_{1.5}Co_{1.5}O_4$ into NiO and $NiCo_2O_4$, or NiO and Co_3O_4, when the annealing temperature gradually increased from 400 to 500 and 600 °C. [13] The TG/DTA differential thermal analyzing results of the as-prepared precursor provided in Fig. S3 also support this observation. A great loss of mass (~24%) was found when the annealing temperature was elevated from ~200 to ~390 °C. The percentage of mass loss is close to the mass change caused by the oxidation and decomposition of $NiCo(OH)_2CO_3$ to form the binary metal oxide $Ni_{1.5}Co_{1.5}O_4$ following the reaction mechanism shown in Fig. 2. When the testing temperature is over 400 °C, the loss of oxygen from the crystal structure of $Ni_{1.5}Co_{1.5}O_4$ to form hybrid oxides of NiO and

$NiCo_2O_4$, and/or Co_3O_4 should be responsible to the observed slight mass loss.

The abovementioned observation are also clearly clarified by the analysis results of EDS element mapping and the HRTEM. As demonstrated in Figs. 6, S4 and S5, the EDX mapping results for O, Co and Ni of NCO-400, NCO-500 and NCO-600, indicate that the Co and Ni components uniformly distribute within the oxide thorns of all NCOs. No obvious segregations of element Ni and Co can be found from NCO-400, NCO-500 and NCO-600. Solo NiO and Co3O4 particles could not be found from NCO-500 and NCO-600 compounds. Furthermore, Figs. 7 and 8 present the high-resolution transmission electron microscope (HRTEM) images, Fourier-filtered image and fast Fourier transformation (FFT) images corresponding to the selected area SA-1 and SA-2 outlined by dashed red line of NCO-600 in Fig. 7a. The high resolution lattice fringe of SA-1 within the lattice spacing of ~0.242 nm and ~0.207 match well with the (111) and (00-2) plane of cubic phase NiO, while the high resolution lattice fringe of SA-2 within the lattice spacing of ~0.468 and ~0.405 nm match well with the (111) and (00-2) plane of cubic phase $NiCo_2O_4/Co_3O_4$. What is more, the corresponding (FFT) patterns of SA-1 and SA-2 are clear regular diffraction spots of cubic phase NiO and $Co_3O_4/NiCo_2O_4$, see Figs. 7d and 8d, respectively. All above observation suggests that the NCO-500 and NCO-600 nanoparticles are comprised of two or multi dispersed phase of NiO, $NiCo_2O_4$ and/or Co_3O_4.

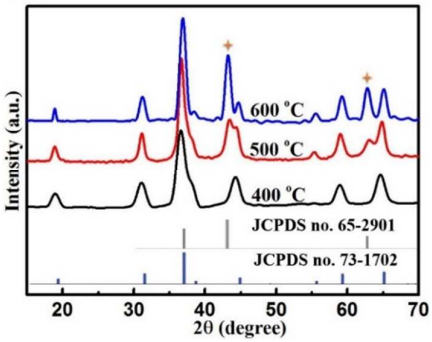

Fig. 5. The X-ray diffraction patterns of hierarchical nickel cobalt oxides NCO-400, NCO-500 and NCO-600, respectively.

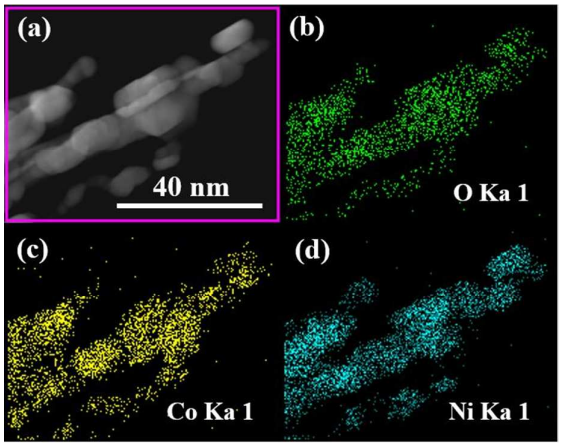

Fig. 6. FE-TEM image (a) and corresponding EDS mapping for O(b), Co(c) and Ni(d) of NCO-600, respectively.

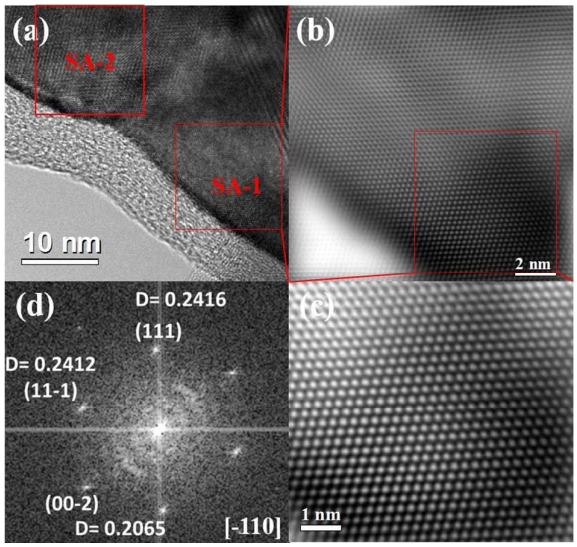

Fig. 7. The high resolution TEM image of NCO-600 (a), Fourier-filtered image (b, c) and FFT image (d) from the selected area SA-1 outlined by dashed red line in (a).

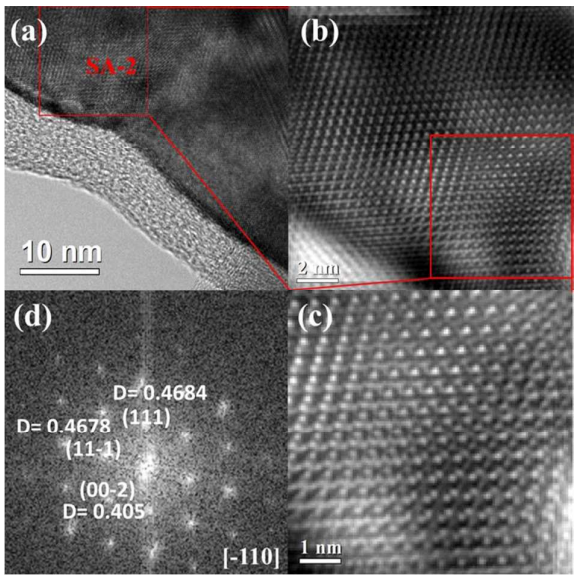

Fig. 8. The high resolution TEM image of NCO-600 (a), Fourier-filtered image (b, c) and FFT image (d) from the selected area SA-2 outlined by dashed red line in (a) and Fig. 7a.

Since the above-mentioned advantages of the nanosized primary particle and the porous structure provide short diffusion distance and large active area for Li^+, the obtained pure phase NCO-400, mutil phase hybrids NCO-500 and NCO-600 nanostructures deliver superior rate capability as advanced anode materials for LIBs, see Figs. 9 and 10. The corresponding charge/discharge profiles cycled at the current density ranged from 180 to 4500 mAg^{-1} are displayed in Fig. 9a, 9b and 9c, which are similar to previous reports. [20] As shown in Fig. 9d, the as-prepared hierarchical $Ni_{1.5}Co_{1.5}O_4$ sphere composed of mesoporous thorn array (NCO-400) delivers a charge capacity of ~1063, ~963, ~874, ~680 and ~280 $mAhg^{-1}$ at the current density of 180, 450, 900, 1800 and 4500 mAg^{-1},

respectively, which are much higher than that of the reported hierarchical flower-like $Ni_{1.5}Co_{1.5}O_4$, ~1000, ~800, ~480 and ~320 $mAhg^{-1}$ at the current density of 200, 400, 800 and 1000 mAg^{-1}, respectively. [20] NCO-500 and NCO-600 deliver slightly low capacity than that of NCO-400 at low rate, but they show better capacity retention ratio than NCO-400 at high rate.

As for the first discharge at a relative low current density of 180 mAg^{-1}, there are three obvious voltage plateaus, which are corresponding to three of two phase transformation. The plateau located at ~1.2 V can be ascribed to the reduction of Ni^{3+} and Co^{3+}, to Ni^{2+} and Co^{2+}, respectively. The redox reactions of this electrochemical process for NCOs is believed to proceed as follows:

$2Ni_{1.5}Co_{1.5}O_4$ (/$2Co_3O_4$)+$4Li^+ + 4e \rightarrow 3NiCoO_2$ (/3CoO) + $2Li_2O$ (1)

As mentioned above, the Ni^{2+} and Ni^{3+} ions are inclined to precipitate out from $Ni_{1.5}Co_{1.5}O_4$ to form NiO phase with the increase of calcination temperature. This observation should be accounted for the descending plateau capacity of NCO-400, NCO-500 and NCO-600, see Fig. 9a, 9b and 9c. According to previous reports, the voltage plateau strated from ~1.0 to ~0.75 V could be attributed to the reduction of Ni^{2+} and Co^{2+} to metallic Ni and Co. The redox reaction of this electrochemical process for NCOs are believed to proceed as follows:

$NiCoO_2$ (NiO + CoO) + $4Li^+ + 4e \rightarrow$ Ni + Co + $2Li_2O$ (2)

Subsequently, when the tested batteries are discharged to a voltage lower than 0.75V in this initial cycle, a catalytic side reaction between metallic Ni, Co and electrolyte can be commonly observed in first discharge process of transition metal oxides. This complex side reaction normally accounts for the large irreversible capacity and low coulombic efficiency. However, the partially reversible reduction and oxidation of electrolyte can be ascribed to the part of capacity over theoretical capacity.[21] As shown in Fig. 9d, the subsequent charge/discharge capacity of NCO-400, NCO-500 and NCO-600 at the current density from 180 to 4500 mAg^{-1} are much higher than the theoretical capacity (~900 $mAhg^{-1}$) calculated based on the redox reaction (1) and (2).

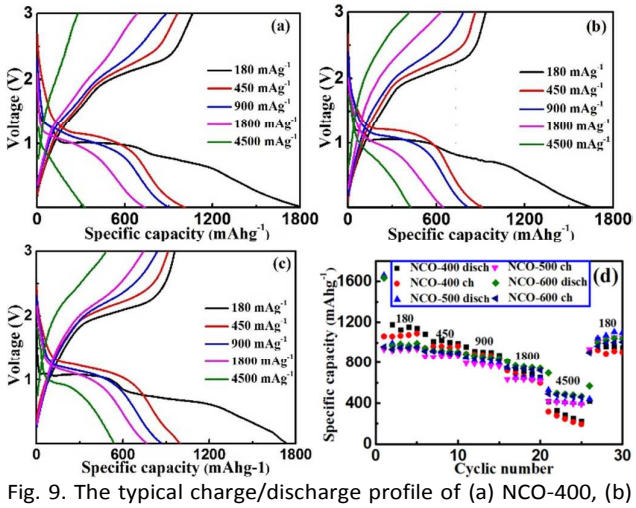

Fig. 9. The typical charge/discharge profile of (a) NCO-400, (b) NCO-500 and (c) NCM-600 at the constant current densities from 180 to 4500 mAg^{-1}.

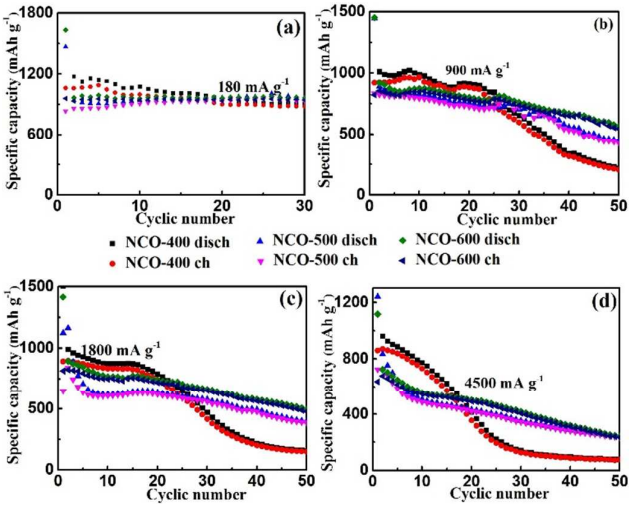

Fig. 10. Discharge/charge cyclic performance of hierarchical thorn spheres NCO-400, NCO-500 and NCO-600 at different current densities of (a) 180 mAg^{-1}, (b) 900 mAg^{-1}, (c) 1800 mAg^{-1}, (b) 4500 mAg^{-1}, respectively.

Moreover, the excellent rate capabilities of all NCOs can be further confirmed by the cyclic test results shown in Fig. 10. The initial charge capacities of NCO-400 are 1063.3, 922.6, 893 and 860 $mAhg^{-1}$ at the current density of 180, 900, 1800 and 4500mAg^{-1}, respectively. The initial capacities of NCO-400 at the current density of 180, 900, 1800 and 4500mAg^{-1} are higher than that of NCO-500/NCO-600, i.e. 835/960, 832.9/824.1, 842.8/815.9 and 725.7/678.9, respectively. The superior rate performance of the as-prepared NCOs should be attributed to the nanosized primary particles and the hierarchical porous morphology, as well as the dispersed hybrid nano phase structure. The slightly descenting capacity of NCO-400, NCO-500 and NCO-600 should be ascribed to the increase amount of NiO component within the obtained hybrid oxides and the decreased specific surface area. Depending on the applied charge/discharge current density, NCO-400 exhibits good cyclic stability in the first 20 or 30 cycles. However, after that, the electrochemical activity of NCO-400 degrades obviously due to the pulverization caused by the large volumetric expansion and the increased irreversible capacity due to decreased particle size and gradually loss of close contact between amorphous metallic Ni/Co with Li_2O. Nevertheless, NCO-600 shows much better cyclic stability than NCO-500 and NCO-400. The great promoted cyclic performance of NCO-600 might be profited from the effectively suppressed side reactions with electrolyte and the alleviated volume change during the charge/discharge process, which should be ascribed to the reduced specific surface area and the dispersed multi-phase hybrid crystal structure of $NiCo_2O_4$/Co_3O_4/NiO resulted from the elevated calcination temperature (500 and 600 °C). Being cycled at 900, 1800 and 4500 mAg^{-1} for 50 cycles, the charge capacity of NCO-600 still kept 545.5, 478.1 and 233.8 $mAhg^{-1}$, respectively. The calculated capacity retention ratios of NCO-600 are 66.1%, 58.6% and 36.7%, respectively.

In summary, the hierarchical $NiCo(OH)_2CO_3$ spheres comprised of thorn arrays have been successfully prepared as precursors by using the hydrothermal method. By annealing the precursors at 400, 500 and 600°C for 2h, the pure phase hierarchical porous spheres composed of porous $Ni_{1.5}Co_{1.5}O_4$ thorn arrays (NCO-400) and comprised of the dispersed multi-phase ($NiCo_2O_4$/Co_3O_4/NiO) hybrid thorn arrays (NCO-500 and NCO-600) were obtained. Since the nanosized primary particle and the special porous hierarchical structure provide short diffusion distance and large active area for Li^+, meanwhile the reduced specific surface area and the dispersed multi-phase hybrid crystal structure of $NiCo_2O_4$/Co_3O_4/NiO resulted from the elevated calcination temperature (500 and 600 °C) could effectively suppress the side reactions with electrolyte and alleviate the volume change during the charge/discharge process, the above-mentioned advantages in turn make the as-prepared hierarchical nickel cobalt oxides (NCO) porous thorn spheres exhibit superior rate capability and promoted cyclic stability. After 50 charge/discharge cycles at 900, 1800 and 4500 mAg^{-1}, the charge capacity of NCO-600 still kept 545.5, 478.1 and 233.8 $mAhg^{-1}$, respectively. Prospectively, the rate capability and cyclic stability could be further promoted by carbon coating or hybrid with graphene or CNTs in future.

This work was supported by National Natural Science Foundation of China (51402155), Priority Academic Program Development of Jiangsu Higher Education Institutions（PAPD）(YX03001), National Synergistic Innovation Center for Advanced Materials (SICAM), Foundation of NJUPT (NY214021).

Notes and references

[a] Key Laboratory for Organic Electronics & Information Displays and Institute of Advanced Materials, Nanjing University of Posts & Telecommunications, Nanjing, 210046, P.R.China. Email: hzd0506127@gmail.com (Z.D Huang);
iamywma@njupt.edu.cn (Y.W. Ma).
[b] Engineering Laboratory for the Next Generation Power and Energy Storage Batteries, Graduate School at Shenzhen, Tsinghua University, Shenzhen, 518055, PR China.
[c] Department of Mechanical and Aerospace Engineering, The Hong Kong University of Science and Technology, Clear Water Bay, Kowloon, Hong Kong, China.

‡ Zhen-Dong Huang and Kun Zhang contributed equally to this work.

1 C.Z. Yuan, H. B. Wu, Y. Xie, X. W. Lou, Angew. Chem. Int. Ed., 2014, 53, 1488.
2 D.W.Xu, Y.B. He, X.D. Chu, Z.J. Ding, B.H. Li, J.F. He, H.D. Du, X.Y. Qin and F.Y. Kang, ChemSusChem, 2015, 8, 1009.
3 L. Yu, L. Zhang, H. B. Wu, G.Q. Zhang and X. W. Lou, Energy Environ. Sci., 2013, 6, 2664.
4 L. Hu, H. Zhong, X.R. Zheng, Y.M. Huang, P. Zhang & Q.W. Chen, Scientific Reports, 2012, 2, 986, DOI-10.1038-srep00986.
5 S. Li, X.Y. Qin, H.R. Zhang, J.X. Wu, Y.B. He, B.H. Li, F.Y. Kang, Electrochem. Commun., 2014, 49, 98–102.
6 X.Y. Zheng, W. Lv, Y.B. He, C. Zhang, W.Wei, Y. Tao, B.H. Li, and Q. H. Yang, J. Nanomater., 2014, 2014, http://dx.doi.org/10.1155/2014/974285.
7 B. Zhang, Y. Yu, Z.D. Huang, Y.B. He, D. Jang, W.S. Yoon, Y.W. Mai, F.Y. Kang and J.K. Kim, Energy Environ. Sci., 2012, 5, 9895.
8 B. Zhang, Q. B. Zheng, Z. D. Huang, S.W. Oh, J.K. Kim, Carbon, 2011, 49, 4524.
9 L.R. Hou , L. Lian, L.H. Zhang , G. Pang , C.Z Yuan , and X.G. Zhang, Adv. Funct. Mater. 2014, DOI:10.1002/adfm.201402827.
10 L.H. Zhang, S.Q. Zhu, H. Cao, G. Pang, J.D. Lin, L.R. Hou, C.Z. Yuan, RSC Adv., 2015,5, 13667.
11 L.Y. Guo, Q. Ru, X. Song, S.J. Hu and Y.D. Mo, J. Mater. Chem. A, 2015, 3, 8683.
12 Y.Q. Zhu, C.B. Cao, J.T. Zhang and X.Y. Xu, J. Mater. Chem. A, 2015, 3, 9556.
13 T. Li, X.H. Li, Z.X. Wang, H.J. Guo and Y. Li, J. Mater. Chem. A, 2015, 3, 11970.
14 M.H. Kim, Y. J. Hong and Y. C. Kang, RSC Adv., 2013, 3, 13110.
15 L.J. Wang, B. Liu, S.H. Ran, L.M. Wang, L.N. Gao, F.Y. Qu, D. Chen and G.Z. Shen, J. Mater. Chem. A, 2013, 1, 2139.
16 Y.R. Liu, B.C. Zhang, J.K. Feng, and S.L. Xiong, RSC Adv., 2015, 5, 26863.
17 L. Zhou, D.Y. Zhao, and X. W. Lou. Adv. Mater., 2012, 24, 745.
18 S. M. Hwang, S.Y. Kim, J.G. Kim, K.J. Kim, J.W. Lee, M.S. Park, Y.J. Kim, M. Shahabuddin, Y. Yamauchi and J.H. Kim, Nanoscale, 2015, 7, 8351.
19 C.C. Fu, G.S. Li, D. Luo, X.S. Huang, J. Zheng, and L.P. Li, ACS Appl. Mater. Interfaces 2014, 6, 2439.
20 Y.H. Jin, L. Wang, Y.M. Shang, J. Gao, J.J. Li, X.M. He, Mater. Lett., 2015, 151, 49.
21 X.L. Zhou, Y.R. Zhong, M. Yang, Q. Zhang, J.P. Wei, and Z. Zhou, ACS Appl. Mater. Interfaces, 2015, 7, 12022.
22 W.H. Ryu, S.J. Lim, W.K. Kim, H. Kwon, J. Power Sources, 2014, 257, 186.
23 Z.Q. Xie, J.Q, Zhao, Y. Wang, Electrochim. Acta, 2015, 174, 1023.

Graphical abstract:

The short diffusion distance and large active area for Li^+, together with the suppressed side reaction and volume change make hierarchical nickel cobalt oxides (NCO) porous spheres comprised of nanoscale thorn arrays with dispersed multi-phase structure exhibit superior rate capability and promoted cyclic stability.